



Repositorio Institucional de la Universidad Autónoma de Madrid

<https://repositorio.uam.es>

Esta es la **versión de autor** del artículo publicado en:

This is an **author produced version** of a paper published in:

Angewandte Chemie - International Edition 54.26 (2015): 7688-7692

DOI: <http://dx.doi.org/10.1002/anie.201501550>

Copyright: © 2015 WILEY-VCH Verlag GmbH & Co. KGaA, Weinheim

El acceso a la versión del editor puede requerir la suscripción del recurso

Access to the published version may require subscription

Combining novel electron-accepting phthalocyanines and nanorod-like CuO electrodes for p-type dye-sensitized solar cells

Oliver Langmar,^[a] Carolina R. Ganivet,^[b] Annkatrin Lennert,^[a] Rubén D. Costa,^[a] Gema de la Torre,^[b] Tomás Torres,^[b] and Dirk M. Guldi^[a]

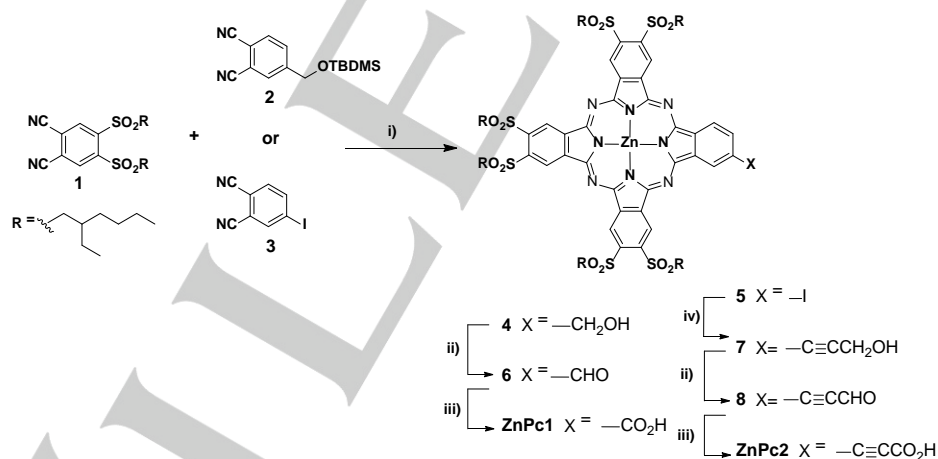
Abstract: In the current work, a novel route for the synthesis of two electron-accepting phthalocyanines featuring linkers with different length as sensitizers for p-type dye-sensitized solar cells are reported. Importantly, our devices – based on novel nanorod-like CuO photocathodes – feature efficiencies of 0.191%, which are to date the highest values ever reported for CuO-based DSSCs.

Current developments in p-type DSSCs focuses on exploring novel electrodes and electron acceptors.^[1,2] Concerning the former, the most prominent material has been nickel(II) oxide (NiO), despite drawbacks such as low transparency, electrode thickness, and low conductivity.^[2] To tackle some of the aforementioned bottlenecks, the preparation of binary NiXO semiconductors, where X is cobalt, have recently evolved as a powerful approach.^[3] A viable alternative is based on the long overlooked copper(II) oxide (CuO), whose films feature higher conductivity, better charge carrier mobility, and comparable valence band energy relative to NiO films.^[4,5] Still, the most recent report on CuO based p-type DSSCs is dated from 2008.^[6] Very likely, state-of-the-art efficiencies as low as 0.011% resulted in a moderate interest. Recent improvements in the field of CuO based p-type DSSCs are due to the use of copper delafossite (CuXO₂) electrodes with X being aluminum, chromium, or gallium.^[7] Higher conductivities as well as lower valence band

energies, which cause higher open-circuit voltages (V_{oc}), represent the major benefits of the latter electrodes. Other CuO nanostructures like, for example, nanorods, nanoplates, etc. have never been explored to date. This is where the current work sets in. In particular, we demonstrate for the first time that DSSCs based on nanorod-like CuO electrodes outperform those with nanoparticle-like CuO and perform in a manner similar to those with CuXO₂.

Concerning dyes for p-type DSSCs, a myriad of different organic and inorganic sensitizers including triphenylamines,^[8] perylene-diimides,^[9] perylene-bithiophene-triphenylamine triads,^[10] porphycenes,^[11] and ruthenium complexes,^[12] have been designed and probed. Notably, porphyrinoids have led to the most efficient n-type DSSCs up to date.^[13,14] Key merits of porphyrins, and specially of their synthetic related phthalocyanines (Pcs),^[15,16] are their exceptional light-harvesting features and their facile functionalization with either electron-donors or electron-acceptors, underlining their potential for DSSCs.

In light of the latter, tuning the physicochemical features of phthalocyanines towards new electron-accepting dyes^[17,18] by means of placing electron-withdrawing substituents at their periphery, complements, in the current work, our research regarding nanorod-like CuO electrodes.^[19]



Scheme 1. Conditions: i) Zn(OAc)₂, o-DCB/DMF (3:1), 170 °C, Ar, 18h; ii) IBX, DMSO/THF; iii) H₃NSO₃/H₂O followed by NaClO₂; iv) propargyl alcohol, Pd(PPh₃)₂Cl₂, CuI, NEt₃, THF

Notably, the synergy of nanorod-like CuO DSSCs and electron-accepting Pcs enables the construction of p-DSSCs with efficiencies as high as 0.103% and 0.191% with iodine- and cobalt-based electrolytes, respectively. The latter represents the highest values ever reported for pure CuO-based DSSCs. The design and the synthesis of two novel zinc phthalocyanines – **ZnPc1** and **ZnPc2** as shown in Scheme 1 – for the sensitization of CuO nanorods are driven by several incentives. Firstly, six electron-withdrawing alkylsulfonyl-groups are attached at the phthalocyanine periphery to render them electron accepting. Secondly, branched rather than linear alkyl chains are used to suppress aggregation on the surface of CuO nanorods. Thirdly,

[a] Oliver Langmar, Annkatrin Lennert, Dr. Rubén D. Costa, and Prof. Dirk M. Guldi
Department of Physical Chemistry and Pharmacy, Interdisciplinary Center for Molecular Materials
University of Erlangen-Nürnberg
Egerlandstr. 3, 91058, Erlangen, Germany
E-mail: ruben.costa@fau.de, dirk.guldi@fau.de

[b] Carolina R. Ganivet, Dr. Gema de la Torre, and Prof. Tomás Torres
Departamento de Química Orgánica
Universidad Autónoma de Madrid
C/Francisco Tomás y Valiente 7, 28049 Madrid, Spain
E-mail: tomas.torres@uam.es
Supporting information for this article is given via a link at the end of the document.

COMMUNICATION

either directly linked – **ZnPc1** – or conjugated – **ZnPc2** – carboxylic acid anchoring groups are attached to facilitate charge injection.

The synthesis of **ZnPc1** and **ZnPc2** is accomplished in several steps in moderate yields – see Scheme 1 and Supporting Information (SI) for more details. Starting from a classical statistical condensation of 4,5-bis(2-ethylhexylsulfonyl)phthalonitrile **1** and either phthalonitrile **2** or **3**, **ZnPcs 4** and **5**, respectively, are obtained.^[20] For **ZnPc1**, two consecutive oxidation steps were necessary to transform the hydroxymethyl **Pc 4** into the corresponding carboxylic acid, namely a reaction with periodinane in DMSO to afford formyl derivative **6** and treatment with NaClO₂ in water in the presence of sulfamic acid. In the case of **ZnPc2**, an initial Sonogashira coupling between monoiodo **5** and propargylic alcohol afforded hydroxypropargyl **Pc 7**. The latter was oxidized following the same two-step procedure mentioned before. All of the final products and their corresponding intermediates were fully characterized by spectroscopic and electrochemical means.

As shown in Figure 1, the absorption and fluorescence spectra of **ZnPc1** and **ZnPc2** are 25 nm red-shifted compared to those seen for a tetra-*tert*-butyl-ZnPc (**ttb-ZnPc**) reference and exhibit slightly lower extinction coefficients. In addition, **ZnPc1** and **ZnPc2** show split Q-bands – see Table S1 – as a result of their asymmetric functionalization.

Next, cyclic voltammetric experiments were performed to probe the electron accepting character of **ZnPc1** and **ZnPc2** – Figure S1. Four quasi-reversible reductions at -0.94, -1.45, -1.82, -2.06 V for **ZnPc1** and at -0.94, -1.36, -1.82, -2.03 V for **ZnPc2** are complemented by one quasi-reversible oxidations at +0.72 V for **ZnPc1** and +0.77 V for **ZnPc2** – all values versus Fc/Fc⁺. When compared with **ttb-ZnPc**, which reveals its lowest reduction at -1.4 V and lowest oxidation at +0.1 V,^[17] **ZnPc1** and **ZnPc2** render better electron acceptors but poorer electron donors. From the aforementioned, we determined LUMO energies for **ZnPc1** and **ZnPc2** of -0.30 V versus NHE.^[21] Considering that the redox potential of the I⁻/I₃⁻ and Co²⁺/Co³⁺ couples are 0.34 and 0.22 V versus NHE,^[22] respectively, **ZnPc1** and **ZnPc2** should be effectively regenerated in p-type DSSCs – Figure S2. Moreover, the low lying HOMOs, that is, +1.36 V (**ZnPc1**) and +1.41 V (**ZnPc2**) versus NHE, implies an efficient electron flow from the valence band (VB) of CuO into the corresponding HOMOs – *vide infra*.

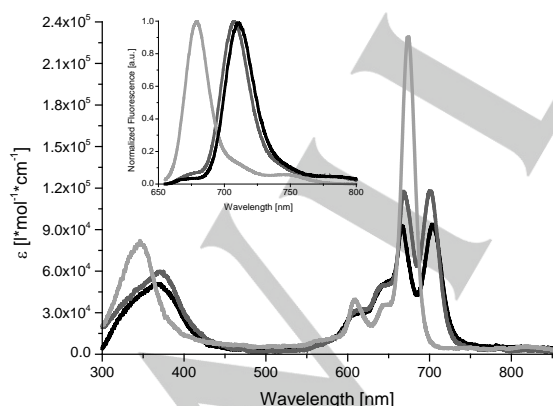


Figure 1. Absorption and fluorescence (inset) spectra of **ZnPc1** (black), **ZnPc2** (dark grey), and **ttb-ZnPc** (light grey) in EtOH (2.3 × 10⁻⁷ M).

Next, we assembled cells consisting of nanorod-like CuO as p-type electrodes and **ZnPc1** / **ZnPc2** as photosensitizers. In particular, electrodes were prepared by doctor-blading a paste of nanorod-like CuO diluted with ethylcellulose in ethanol followed

by sintering at 300°C – see SI for more details.^[23] Crack-free mesoporous morphology and rod-like shapes of CuO after calcination were corroborated by scanning electron microscopy – Figure S3. The Fermi level energy of 0.55 V was determined in Kelvin Probe microscopic experiments. As an approximation, we used the latter in agreement with the literature as the VB energy.^[24] Furthermore, diffuse reflectance assays were used to determine a band-gap energy (E_g) of around 1.61 eV – Figure S4.^[25] With this information in hand, we calculated the energy position of the conduction band (CB) via $E_{CB} = E_{VB} - E_g$ as -1.06 V vs. NHE. Figure S2 illustrates an energy diagram, in which the use of our **ZnPc1** and **ZnPc2** in p-type DSSCs is illustrated. Firstly, the HOMOs are placed 0.81 V (**ZnPc1**) and 0.86 V (**ZnPc2**) below the VB of the electrode. Such driving forces ensure an efficient electron flow from the electrodes to the photoexcited ZnPs. Secondly, upon excitation, recombinations between the LUMOs and the CB is unlikely. Finally, the electrolyte levels are 0.5 to 0.6 V below those of the corresponding LUMOs – *vide supra* – ensuring efficient dye regeneration. P-type DSSCs were completed with Pt as counter electrodes and either with LiI/I₂ (1 M:0.4 M) in a 50:50 (v/v) mixture of acetonitrile/3-methoxypropionitrile or with Co²⁺/Co³⁺ (0.01 M:0.1 M) of [Co(dtb-bpy)₃][PF₆]_{2/3} in acetonitrile as electrolytes – see SI for details.

The photocurrent density versus applied voltage (J-V) and the incident photon-to-current efficiency (IPCE) spectra are shown in Figures 2 and 4, respectively, and the figures-of-merit are gathered in Table 1. The time dependences of the adsorption kinetics are important. For example, the efficiency (η) starts to rise before plateauing at around 60 minutes of **ZnPc** uptake – Figure S5. The same trends are observed for the short-circuit current densities (J_{sc}) and the open-circuit voltages (V_{oc}). Similar concentrations of 1.38 × 10⁻⁸ and 1.39 × 10⁻⁸ M/cm² were derived for **ZnPc1** and **ZnPc2**, respectively, in desorption experiments, which ensures comparability of the figures-of-merit.

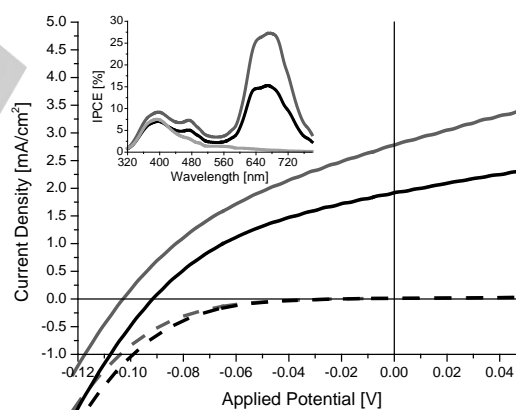


Figure 2. Current density versus applied potential under 1 sun and AM 1.5 (solid line) and dark (dashed line) conditions for **ZnPc1** (black) and **ZnPc2** (dark grey) devices with iodine-based electrolyte. Inset - IPCE spectra of both kind of devices compared to a non-sensitized cell (light grey).

As starting point, we probed I⁻/I₃⁻ devices under 1 sun illumination and AM 1.5 conditions. **ZnPc2** devices show higher V_{oc} s and J_{sc} s than **ZnPc1** devices – please compare 102 with 93 mV and 2.78 with 1.93 mA/cm². In contrast, the fill factors (FF) were nearly the same, leading to overall efficiencies of 0.103% and 0.067% for **ZnPc2** and **ZnPc1**, respectively. In line with the aforementioned, the IPCE values are around 78% higher for **ZnPc2** (27.4%) compared to **ZnPc1** (15.4%) at 670 nm. It is interesting to note that the overall efficiency trend is in line with that observed in n-type DSSCs sensitized by electron-donating ZnPs featuring the same carboxylic linkers.^[16]

COMMUNICATION

Comparable conditions, in terms of dye loading, electrode thickness, and electrolyte composition, as well as differences in J_{sc} s and IPCEs point to a linker-dependent injection and/or recombination processes. **ZnPc2** features the carboxylic linker connected via a carbon-carbon triple bond, while the linker is directly connected in **ZnPc1** – see Scheme 1. In general, the nature of the linker determines both the dye-electrode distance and the orientation of the dye relative to the surface.^[26] Both seem to govern the injection and recombination kinetics, while thermodynamic differences between **ZnPc1** and **ZnPc2** are ruled out – *vide supra*.

Table 1. Device performance under 1 sun and AM 1.5 conditions for **ZnPc1** and **ZnPc2**.

Dye/Electrolyte	V_{oc} [mV]	J_{sc} [mA/cm ²]	FF	η [%]	IPCE [%] at 670nm
ZnPc1 / I ⁻ /I ₃ ⁻	93	1.93	0.38	0.067	15.4
ZnPc2 / I ⁻ /I ₃ ⁻	102	2.78	0.36	0.103	27.4
ZnPc1 / Co ²⁺ :Co ³⁺	224	1.99	0.32	0.141	14.9
ZnPc2 / Co ²⁺ :Co ³⁺	251	2.35	0.32	0.191	20.5

Considering the CuO electrode opaqueness we turned to electrochemical impedance spectroscopy (EIS). Applying different voltages to change between short-circuit current density and open-circuit voltage conditions assists in probing the aforementioned processes in p-type DSSCs.^[27,28] As an illustration, the Nyquist plots under V_{oc} and J_{sc} conditions are shown in Figure S6. Here, two semicircles, which relate to the resistance across the platinum/electrolyte interface in the high frequency region and the dye/electrode/electrolyte interface in the low frequency region are discernable.^[27] From the corresponding electrical circuit model, which is illustrated in Figure S7, the resistances and capacitances are derived – Figure 3 and Table S2.

EIS measurements under dark conditions give insights into recombination processes between the electrode and the electrolyte.^[27] Figure 3 documents that the recombination resistance (R_{rec}) increases with decreasing voltage. Within the voltage range, slightly lower resistances towards recombination with the I⁻/I₃⁻ redox couple are noted for **ZnPc2** devices. In the latter, larger dye to electrode distances facilitate interactions with the redox couple, as the electrode surface is more exposed to the polyiodide species. A closer look at the IPCE spectra in Figure 2 substantiates this trend. Here, **ZnPc2** devices feature in the high-energy region, which is dominated by excitation of CuO and/or the redox couple, slightly higher IPCEs ($\leq 2\%$) compared to devices made of **ZnPc1**.

EIS measurements under illumination illustrate that several different contributions impact the charge-transfer resistance (R_{CT}). Besides electrode to electrolyte recombination processes, charge injection from the electrode to the dye and charge transport throughout the electrode play major roles.^[29] Again, a linear increase of R_{CT} with decreasing voltage is noted before it plateaus at around J_{sc} conditions – Figure 3. A similar trend has recently been reported for NiO-based DSSCs.^[28]

Overall, **ZnPc2** devices give rise to lower R_{CT} s throughout the entire voltage range relative to **ZnPc1** devices, indicating better charge injection and charge transport in the former. At V_{oc} conditions, the recombination across the electrode/electrolyte interface dominates due to the lack of external currents. In line with EIS observations in the dark, the resistance towards recombination with I⁻/I₃⁻ is lower for **ZnPc2** (40.0 Ω) than for **ZnPc1** (61.8 Ω). At J_{sc} and under forward conditions, the absence of recombinations enables establishing the relation between R_{CT}

and the charge injection, that is, from the electrode to the dye. From a comparison between **ZnPc1** (506.3 Ω) and **ZnPc2** (266.4 Ω), a nearly two times lower R_{CT} prompts to better charge injection for the latter. The IPCE spectra are helpful in this regard, since photocurrents at around 670 nm – due to dye excitation – are nearly twice as high for **ZnPc2**. The lack of photoactivity of the electrolyte in the low-energy region only leaves contributions from the charge injection to rationalize the superior performance of devices featuring **ZnPc2**.

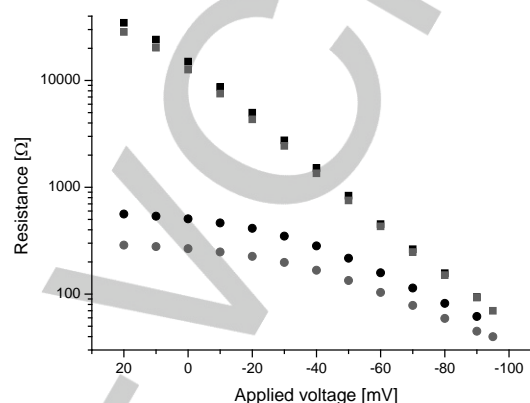


Figure 3. Resistance versus applied voltage for **ZnPc1** (black) and **ZnPc2** (grey) devices under dark (squares) and illumination (circles) conditions.

Additional device properties, namely the chemical capacitance (C_{μ}), the charge collection efficiency (η_{cc}), the effective diffusion length (L_{eff}), and the effective diffusion coefficient (D_{eff}) have been determined for all devices and are summarized in Figure S8.^[28,30] Briefly, C_{μ} directly correlates with the density of injected holes at the electrode. A higher rate of charge injection increases the hole density, affording higher V_{oc} and C_{μ} .^[31] In agreement with this notion is the fact that higher V_{oc} s, higher C_{μ} s, and superior charge injections were observed for **ZnPc2**. This also explains the improved η_{cc} s in devices with **ZnPc2**, since charge injection across the electrode/dye interface is twice as efficient. This is also reflected in longer L_{eff} s and higher D_{eff} s compared to **ZnPc1** devices.

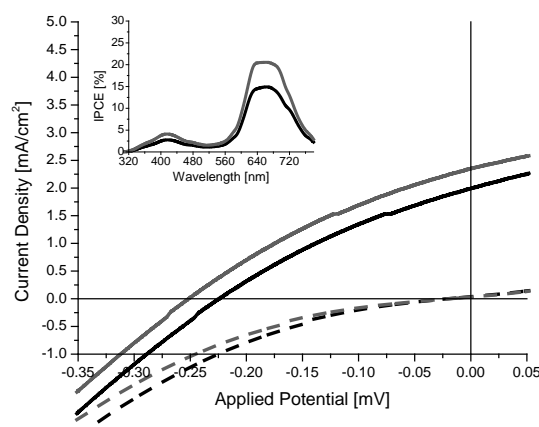


Figure 4. Current density versus applied potential under 1 sun and AM 1.5 (solid line) and dark (dashed line) conditions for **ZnPc1** (black) and **ZnPc2** (grey) devices with cobalt-based electrolyte. Inset - IPCE spectra for both kind of devices. Please note that the IPCE of the non-sensitized device is not shown, since a maximum of only 0.13% at 400 nm was measured.

The major bottleneck of our devices evolves around the low V_{oc} , since J_{sc} s are comparable to Cu_2O based DSSCs.^[7] Using cobalt di-*tert*-butyl bipyridine hexafluorophosphate $[Co(dtb-bpy)_3][PF_6]_{2/3}$ as electrolyte is the most efficient way to overcome this limitation.^[22] Under 1 sun illumination and AM 1.5 conditions, **ZnPc2** DSSCs reveal higher V_{oc} s and J_{sc} s (251 mV and 2.35 mA/cm²) than **ZnPc1** DSSCs (224 mV and 1.99 mA/cm²) – Figure 4 and Table 1. Importantly, IPCEs for **ZnPc2** at 670 nm are nearly 5.5% higher than for **ZnPc1**. More relevant, V_{oc} s increase by almost 150% when comparing cobalt-based devices with iodine-based devices leading to η s of 0.191% for **ZnPc2** and 0.141% for **ZnPc1**. EIS assays under V_{oc} and J_{sc} conditions are also in line with the trends noted for devices with iodine-based electrolytes – Figure S9 and Table S3. **ZnPc2** devices reveal in comparison to **ZnPc1** ones a slightly higher recombination with the electrolyte, as well as a better charge injection.

In conclusion, two novel electron accepting ZnPs – **ZnPc1** and **ZnPc2** – which differ in their linker length, were synthesized and characterized by means of steady-state photophysical as well as electrochemical techniques. Both ZnPs present significant absorption cross sections throughout the visible part of the solar spectrum and excellent electron accepting behavior. These features prompted us to use them as photosensitizers in p-DSSCs based on nanorod-like Cu_2O electrodes, which have never been explored. To this end, devices featuring **ZnPc1** and **ZnPc2** were measured under either 1 sun and AM 1.5 conditions or dark conditions, yielding maximum efficiencies of up to 0.103% and 0.191% for iodine- and cobalt-based electrolytes, respectively. These values represent the highest ever reported efficiencies for pure Cu_2O p-type DSSCs. Furthermore, EIS assays corroborate that **ZnPc2**, featuring a carboxyethynyl anchor is a more suitable photosensitizer than **ZnPc1**, in which the carboxylic acid anchor is directly linked to the macrocycle. The presence of the ethynyl bridge enhances the electronic coupling between ZnPc and Cu_2O , providing an optimum balance between charge injection and charge recombination. Future research will be focused on further optimization and EIS characterization of p-type Cu_2O devices, as well as the improvement of electron-accepting ZnPs for p-type DSSC applications.

Acknowledgements

The authors thank the German Science Council (DFG) for the financial support in the framework of the Cluster of Engineering of Advanced Materials (EAM), the MINECO Spain (CTQ2014-52869/BQU), the Comunidad de Madrid Spain (FOTOCARBON, S2013/MIT-2841), and the European Union within the FP7-ENERGY-2012-1 nr. 309194-2, GLOBALSOL.

Keywords: Acceptor zinc phthalocyanines • Cu_2O nanorods • Cu_2O electrodes • p-type DSSC • Electrochemical impedance spectroscopy

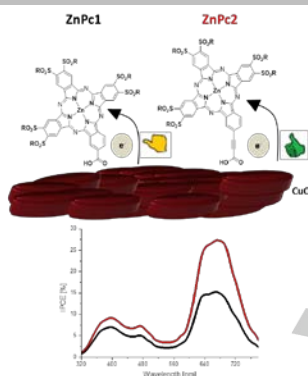
- [1] F. Odobel, L. Le Pleux, Y. Pellegrin, E. Blart, *Acc. Chem. Res.* **2010**, *43*, 1063–1071.
- [2] F. Odobel, Y. Pellegrin, *J. Phys. Chem. Lett.* **2013**, *4*, 2551–2564.
- [3] G. Natu, P. Hasin, Z. Huang, Z. Ji, M. He, Y. Wu, *ACS Appl. Mater. Interfaces* **2012**, *4*, 5922–5929.
- [4] D. M. Jundale, P. B. Joshi, S. Sen, V. B. Patil, *J. Mater. Sci. Mater. Electron.* **2012**, *23*, 1492–1499.
- [5] S. Makhlof, M. Kassem, M. Abdel-Rahim, *J. Mater. Sci.* **2009**, *44*, 3438–3444.
- [6] S. Sumikura, S. Mori, S. Shimizu, H. Usami, E. Suzuki, *J. Photochem. Photobiol. A Chem.* **2008**, *194*, 143–147.
- [7] M. Yu, T. I. Draskovic, Y. Wu, *Phys. Chem. Chem. Phys.* **2014**, 5026–5033.
- [8] P. Qin, H. Zhu, T. Edvinsson, G. Boschloo, A. Hagfeldt, L. Sun, *J. Am. Chem. Soc.* **2008**, *130*, 8570–8571.
- [9] L. Le Pleux, A. L. Smeigh, E. Gibson, Y. Pellegrin, E. Blart, G. Boschloo, A. Hagfeldt, L. Hammarström, F. Odobel, *Energy Environ. Sci.* **2011**, *4*, 2075–2084.
- [10] M. Weidelener, A. Mishra, A. Nattestad, S. Powar, A. J. Mozer, E. Mena-Osteritz, Y.-B. Cheng, U. Bach, P. Bäuerle, *J. Mater. Chem.* **2012**, *22*, 7366–7379.
- [11] S. Feihl, R. D. Costa, W. Brenner, J. T. Margraf, R. Casillas, O. Langmar, A. Browa, T. E. Shubina, T. Clark, N. Jux, et al., *Chem. Commun.* **2014**, 50, 11339–11342.
- [12] Z. Ji, G. Natu, Y. Wu, *ACS Appl. Mater. Interfaces* **2013**, *5*, 8641–8648.
- [13] M. Urbani, M. Grätzel, M. K. Nazeeruddin, T. Torres, *Chem. Rev.* **2014**, *114*, 12330–12396.
- [14] S. Mathew, A. Yella, P. Gao, R. Humphry-Baker, B. F. E. Curchod, N. Ashari-Astani, I. Tavernelli, U. Rothlisberger, M. K. Nazeeruddin, M. Grätzel, *Nat. Chem.* **2014**, *6*, 242–247.
- [15] J.-J. Cid, J.-H. Yum, S.-R. Jang, M. K. Nazeeruddin, E. Martínez-Ferrero, E. Palomares, J. Ko, M. Grätzel, T. Torres, *Angew. Chemie* **2007**, *119*, 8510–8514.
- [16] M.-E. Ragoussi, J.-H. Yum, A. K. Chandiran, M. Ince, G. de la Torre, M. Grätzel, M. K. Nazeeruddin, T. Torres, *Chem. Phys. Chem.* **2014**, *15*, 1033–1036.
- [17] M.-E. Ragoussi, G. Katsukis, A. Roth, J. Malig, G. de la Torre, D. M. Guldi, T. Torres, *J. Am. Chem. Soc.* **2014**, *136*, 4593–4598.
- [18] A. Roth, M.-E. Ragoussi, L. Wibmer, G. Katsukis, G. de la Torre, T. Torres, D. M. Guldi, *Chem. Sci.* **2014**, *5*, 3432–3438.
- [19] B. Tylleman, G. Gbabode, C. Amato, C. Buess-Herman, V. Lemaire, J. Cornil, R. Gómez Aspe, Y. H. Geerts, S. Sergeyev, *Chem. Mater.* **2009**, *21*, 2789–2797.
- [20] Please notice that for the synthesis of **4** a deprotection step is necessary after the cyclotramerization reaction. For details see SI.
- [21] C. M. Cardona, W. Li, A. E. Kaifer, D. Stockdale, G. C. Bazan, *Adv. Mater.* **2011**, *23*, 2367–2371.
- [22] E. A. Gibson, A. L. Smeigh, L. Le Pleux, L. Hammarström, F. Odobel, G. Boschloo, A. Hagfeldt, *J. Phys. Chem. C* **2011**, *115*, 9772–9779.
- [23] S. Ito, T. N. Murakami, P. Comte, P. Liska, C. Grätzel, M. K. Nazeeruddin, M. Grätzel, *Thin Solid Films* **2008**, *516*, 4613–4619.
- [24] C.-Y. Chiang, K. Aroh, N. Franson, V. R. Satsangi, S. Dass, S. Ehrman, *Int. J. Hydrogen Energy* **2011**, *36*, 15519–15526.
- [25] V. Kumar, S. K. Sharma, T. Sharma, V. Singh, *Opt. Mater. (Amst.)* **1999**, *12*, 115–119.
- [26] A. S. Hart, C. B. KC, H. B. Gobeze, L. R. Sequeira, F. D'Souza, *ACS Appl. Mater. Interfaces* **2013**, *5*, 5314–5323.
- [27] Z. Huang, G. Natu, Z. Ji, P. Hasin, Y. Wu, *J. Phys. Chem. C* **2011**, *115*, 25109–25114.
- [28] Z. Huang, G. Natu, Z. Ji, M. He, M. Yu, Y. Wu, *J. Phys. Chem. C* **2012**, *116*, 26239–26246.
- [29] H. Choi, S. O. Kang, J. Ko, G. Gao, H. S. Kang, M.-S. Kang, M. K. Nazeeruddin, M. Grätzel, *Angew. Chemie. Int. Ed.* **2009**, *48*, 5938–5941.
- [30] M. Adachi, M. Sakamoto, J. Jiu, *J. Phys. Chem. B* **2006**, *110*, 13872–13880.
- [31] J. Bisquert, *Phys. Chem. Chem. Phys.* **2003**, *5*, 5360–5364.

Entry for the Table of Contents

Layout 1:

COMMUNICATION

The longer the better: Novel electron accepting zinc phthalocyanines, which feature different linker lengths, in combination with nanorod-like CuO electrodes yield efficiencies of up to 0.191% in p-type DSSCs.



Oliver Langmar, Carolina R. Ganivet,
Annkatrin Lennert, Rubén D. Costa,
Gema de la Torre, Tomás Torres, and
Dirk M. Guldi*

Page No. – Page No.
Combining novel electron-accepting zinc
phthalocyanines and nanorod-like CuO
electrodes for p-type dye-sensitized solar
cells